Hindawi
Shock and Vibration
Volume 2021, Article ID 5554379, 16 pages
https://doi.org/10.1155/2021/5554379

Research Article

Dry Friction Interblade Damping by 3D FEM Modelling of Bladed Disk: HPC Calculations Compared with Experiment

Luděk Pešek, Pavel Šnábl, and Vítězslav Bula

Institute of Thermomechanics of the CAS, v.v.i., Prague 182 00, Czech Republic

Correspondence should be addressed to Luděk Pešek; pesek@it.cas.cz

Received 12 February 2021; Accepted 16 September 2021; Published 14 October 2021

Academic Editor: Miguel de Matos Neves

Interblade contacts and damping evaluation of the turbine bladed wheel with prestressed dry friction contacts are solved by the 3D finite element method with the surface-to-surface dry friction contact model. This makes it possible to model the space relative motions of contact pairs that occur during blade vibrations. To experimentally validate the model, a physical model of the bladed wheel with tie-boss couplings was built and tested. HPC computation with a proposed strategy was used to lower the computational time of the nonlinear solution of the wheel resonant attenuation used for damping estimation. Comparison of experimental and numerical results of damping estimation yields a very good agreement.

1. Introduction

The trend in the development of power turbines and jet engines is to continuously improve performance and energy efficiency. Modern turbines are designed for higher operating temperatures and flow rates. The rotating turbine blades are, apart from the considerable centrifugal forces, subjects to aerodynamic forces from the flowing medium. However, the trend of producing ever-longer and ever-thinner blades leads to lower dynamic stiffness. Therefore, dynamic stiffness and structural damping must be increased by additional structural elements, e.g., tie-bosses and shroud connections, with minimal impact on blade weight and aerodynamic loss.

Although the turbines and their bladings can be carefully designed, it is not possible to omit resonant vibration leading to a high-cycle fatigue risk. The bladed wheel with sufficient dissipation of mechanical energy is the protection against this case. Since the material damping of the metal blades is very low, it is necessary to increase the damping by additional construction damping.

Therefore, dry friction damping contacts in tie-bosses, shrouds, or platforms are introduced into the turbine design. In literature, study cases either on blade-to-blade contacts in shrouds or tie-bosses, e.g., Pešek et al. [1], Bachschmid et al. [2], Gu et al. [3], and Santhosh et al. [4], or on blade-to-disk contacts in platforms, e.g., in works of Petrov and Evins [5, 6], Botto et al. [7], Gola and Liu [8], Zucca and Firrone, [9], and Pesaresi et al. [10], can be found.

In general, the contact problems of elastic bodies, Herz's theory is the basis for analytical solutions of contact problems till today. Initial studies on finite element methods regarding contact problems appeared in the 1970s (e.g., Francavilla [11]). Since then, abundant literature on linear and nonlinear contact scenarios within the FEM has appeared (e.g., Wriggers et al. [12] and Simo Laursen [13]).

The effect of the friction damping on the dynamic behavior of the blading is a complex problem of continuum mechanics as to the dynamic behavior of spatial distorted blades coupled by disk and time-variant boundary conditions at contacts with friction (Sextro [14]). It leads to multipoint contacts influenced by production accuracy and roughness of the contact surfaces and thermomechanical coupling (Awrejcewicz and Pyr'yev [15]).

To get the time effective solution of bladed wheels with dynamical dry friction contact, the model can be simplified by (a) reducing a number of DOFs of the blades and disk or (b) linearization or another approximation of the contact. To the group (a) belonged semianalytical solutions with few degrees of freedom, e.g., Bachschmid et al. [2], Pešek et al.

[16], Pennacchi et al. [17], and Pešek and Půst [18]. Furthermore, in models, where a number of DOFs are reduced by model reduction methods, e.g., modal condensation method, the nonlinearity remains only in contacts (Pešek et al. [19] and Zeman et al. [20]).

The methods of the group (b) are represented mainly by the harmonic balance method (HBM) (Magnus and Schwingungen [21]) used for the stationary harmonic vibration analysis. The HBM is very well theoretically developed and widely used in the bladed disc dynamics with friction contacts (e.g., Zmitrowicz [22], Pierre et al. [23], Ferri and Dowell [24], Petrov and Ewins [25, 26], Santliturk et al. [27], Sanliturk et al. [27], and Suss et al. [28]).

The simplified approaches of solution are computational efficient, but they have their drawbacks and limitations due to the simplifications. Namely, for the HBM method, it is necessary to know in advance the contact areas and stiffness used to calculate the contact forces, which requires further demanding experiments (Schwingshackl [29]) or numerical simulations (Voldřich et al. [30]).

The works based on computational contact mechanics using the 3D finite element technology, e.g., Bachschmidt et al. [31], Yamashita et al. [32], Pešek et al. [33–35], and Drozdowski et al. [36], solve this problem as a fully coupled mechanical system with nonholonomic constrains. Friction is herein described by the general Coulomb law, where friction coefficient is a function of a relative velocity and quality of surfaces. The contact forces are here computed by, e.g., penalty, Lagrangian, or augmented Lagrangian methods. These methods are usable for general dynamic excitation with smooth and nonsmooth contact surfaces.

This solution is time consuming leading to high performance computations (HPC), but it is straightforward in the contact description for 3D body motions considering variable contact states in space and time. And with the fast increasing performance of computers, i.e., number of cores and speed of processors, it becomes more and more feasible to everyone. Due to possible space and time discretization inaccuracies and numerical errors, an experimental validation is still needed. Nevertheless, it brings new promising possibilities for solving the dynamics of bladed wheels in addition to the simplified models.

The study deals with our latest research aimed at dry friction damping in the tie-boss contacts (Pešek et al. [37–39]), where bladed wheel systems are numerically described by the 3D finite element method with dynamical contact problem. The works [37–39] present the results of this solution at its early stage. This study brings newly achieved numerical and experimental results of the wheel dynamics for larger amplitudes. It provides new information about the method accuracy when blades reach more dangerous amplitudes of vibration.

Smooth surfaces with high contact stiffness are assumed. Due to the spatially different deformations of the blades during oscillations, there are spatial, relative movements of the contact surfaces creating time-varying contact states in terms of contact area location and contact normal force.

The decisive factor for the suppression of dangerous vibrations is the frictional damping after the transition from microslip contact (stick-slip) motions to macroslips when slip states prevail. As proven experimentally, with macroslips in contacts, the dynamic behavior of the blades approaches the behavior of the blades with open contacts, and conversely under microslips, their behavior approaches the state of blades with bonded contacts. In the second case, accuracy of results is due to precise computations of elastic deformations in contacts very sensitive to the contact modelling (Segalman et al. [40]) and is not herein considered.

For experimental study of the topic and validation of the numerical results, the physical model of the bladed disk with interblade tie-boss contacts has been designed and manufactured. For numerical analysis, the corresponding three-dimensional FE model with friction contacts has been developed in the program ANSYS. The numerical model is built from hexahedral structural finite elements. As for the contacts, the "surface-to-surface" dry friction contact model is applied, and the augmented Lagrangian method is used to compute contact normal pressures and friction stresses. The friction coupling is modelled by the isotropic Coulomb's law.

This solution leads, however, to high performance computations (HPC). Therefore, we used the supercomputer Salomon in the Centre IT4Innovation with 2PFLOPS Rpeak using 24 processors per 5 nodes. The long computational time is caused especially by number of iterations in each integration time step in a large number of nonlinear couplings (30 contact pairs in our case) between discretized contact surfaces. Due to nonlinear solution of the dynamics and therefore long computation time, a computational strategy for more effective damping evaluation was proposed.

In the study, first, the physical model of the bladed wheel and its numerical discretization is described. Second, the numerical linear model of the bladed wheel is validated by modal analysis. Furthermore, the description and results of experimental rotary tests used for comparison with numerical results are presented. We focused on two critical wheel speeds with different modes of vibration, i.e., modes with 2 and 6 nodal diameters (ND). Following is the numerical modelling of the contacts and the computational strategy, and finally, the results of the calculation and comparison with the rotation experiment are discussed.

1.1. Blade Model Design and FE Discretization. The model disk is equipped with 30 prismatic blades. Figure 1 shows the design of bladed wheel with "tie-boss" couplings and additional weights. Each blade is fixed to the disk by the system of two small finger consoles. The bottom console is bolted to the disk, and upper console is bolted to the blade. The consoles are bolted together, and their mutual position is set at 45° angle before they are bolted together. At the tip of the blades, an additional mass is bolted. Each blade flexurally oscillates in the plane α_0 perpendicular to the plane of the blade. The tie-bosses are shoulders, and their ends are in contact at neighboring blades. The shoulders of tie-bosses have the same length, and their placement is at a radius

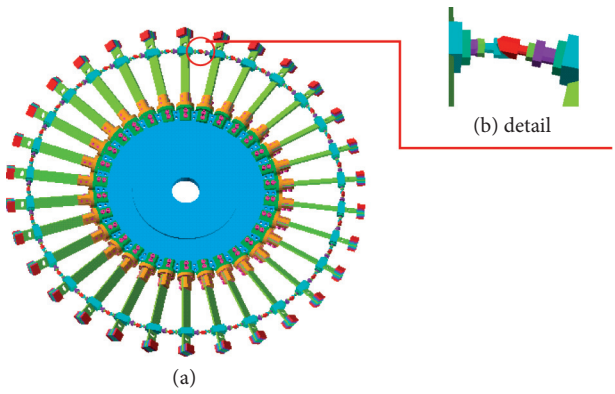

Figure 1: Bladed wheel model with interblade tie-boss couplings. Figure 1 is reproduced from [37].

0.44 m of the wheel. To allow the blade to move freely during flexural vibrations, the ends of the tie-boss shoulders were designed to be at a certain angle.

The definition of cutting planes β_A and β_B of two contacts A and B is schematically shown in Figure 2. The axis ζ_A and ζ_B, respectively, are radials laying in the middle plane of the wheel, starting from the centre of the wheel and passing through the middle between the blades. Therefore, they are 12° apart. If we consider the auxiliary planes α_A and α_B perpendicular to the plane of the wheel and passing through the radials ζ_A and ζ_B, then by rotating them by an angle of 45° around the axes ζ_A and ζ_B, we obtain the cutting planes β_A and β_B. Because of setting up the contact surfaces between the tie-bosses of the neighboring blades, the tie-bosses consist of extensible shoulders screwed with left (right side) and right (left side shoulder) winding into the suspension bolt that was fixed to the blade by two nuts. By screwing the bolt onto the nuts, the shoulders extend simultaneously on both sides.

The three-dimensional FE model of the bladed wheel with tie-bosses (Figure 3(a)) was developed in the program ANSYS 19.3. In total, 89,000 hexahedral eight-node SOLID85 elements were applied for blade and disk discretization. The detail of the mesh at tips of blades B_A, B_B, and B_C is depicted in Figure 3(b). For evaluation of the relative motions of the contact surfaces, two contact pairs A and B were chosen having two nodes N167179, N166940 and N165136, N32610, respectively, that lie in the midst of each contact surface (Figure 3). To validate linear dynamic behavior of the bladed wheel, the contact surfaces of neighboring tie-bosses were in state OPEN. The wheel was clamped in the hub for the dynamic calculations. The global reference system x, y, z of the model coordinates is shown in Figure 3(a).

2. Rotary Tests and Results

2.1. Test Rig Set-Up. Experimental tests under rotation were performed on the rotary test stand of the Institute of Thermomechanics (Figure 4). The model wheel is driven by the three-phase synchronous engine ABB (10 kW) supplied by a current from the frequency converter ACSM1. The

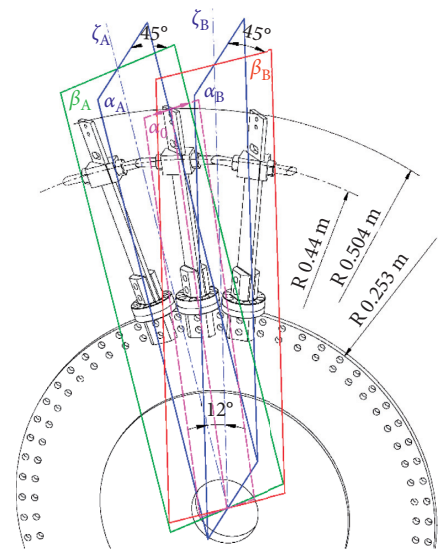

Figure 2: Scheme of the cutting planes of contact surfaces.

scheme of the rig with denotation of components of the wheel, excitation, and measurement is graphically shown in Figure 5.

The rotating bladed wheel is excited by eight electromagnets EM1 ÷ EM8 distributed along the circumference of the wheel. Strain gauge (SG_1) was glued on the blade L1 for measurement of the blade vibration. The absolute encoder ECN1313 (512 lines) was used for the blade position and angular speed detections. Electromagnets were grouped into pairs (EM1, EM5), (EM2, EM6), (EM3, EM7), and (EM4, EM8) for more uniform distribution of the excitations on the wheel. Algorithms for synchronized electromagnetic excitation with revolution were developed in a Simulink program for the real-time control system dSPACE. The normal contact force was realized by prestressed rubber band springs with magnitude 2 N.

2.2. Modal Analysis of Full Bladed Disk. To attune the material parameters of the numerical model, the experimental modal analysis of the full bladed disk was performed for open contacts in a steady nonrotational state. The system Pulse, B&K, and MeScope and Vibrant Technology (Table 1) were used for measurement and analysis. The experimental SIMO modal analysis was evaluated from the axial responses of all blades on the swept sine excitation of the wheel. The eigenfrequencies were classified according to a number of nodal diameters (ND) of the associated eigenmodes.

As it can be seen from the table, the pairs of very close eigenfrequencies for each ND eigenmode appear. It corresponds to the split double eigenfrequencies of the eigenmodes of the rotational bodies with lightly disturbed symmetry. The numerical model with open contacts (Figure 3) was tuned to the experimental results of modal analysis. The eigenfrequencies of modes from 2ND up to 6ND of both numerical and experimental modal analyses are presented in Table 1 and show good agreement. The eigenfrequencies of the numerical open contact model

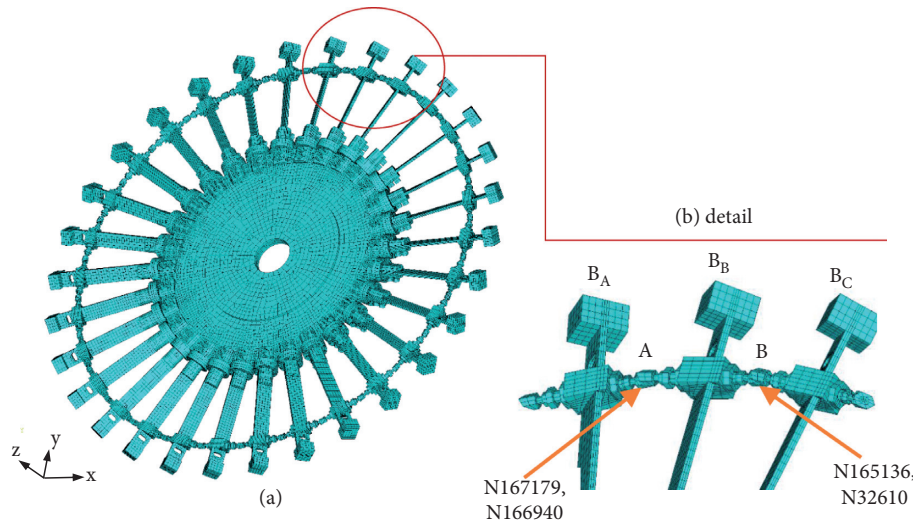

Figure 3: (a) FE mesh of the bladed model with excitation forces FE. (b) Tip detail of three blades with contact pairs A, B and node numbers in the midst of the surfaces.

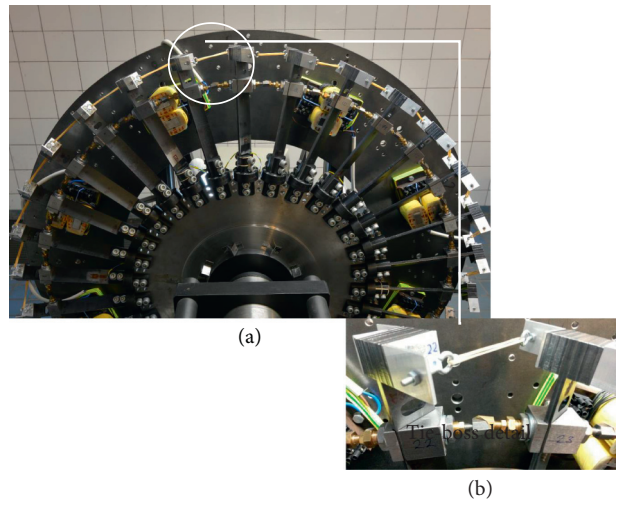

Figure 4: Test rig views. (a) The bladed wheel with tie-boss interconnections. (b) Tie-boss view (detail) with prestress strings. Figure 4 is reproduced from [37].

monotonously increase with a number of ND, and its value converges to a limit eigenfrequency 50.3 Hz for 15ND mode that is close to the first flexural mode of a clamped blade.

Since the open contact model approximates the "eigenfrequency" of the wheel at macroslips, the validation of the numerical modal model is a necessary step before transient nonlinear calculations with dry friction contacts.

2.3. Tests under Revolution. To determine the resonant states of the wheel model under revolution, the Campbell diagrams were evaluated from the strain gauge signal of one blade (L1). The diagram of Figure 6 was ascertained for the bladed wheel with prestressed contacts in tie-bosses. This colored map of amplitude-frequency dependences on revolutions was performed in the automatized data acquisition system PULSE, B & K at a slow run-up (60 up to 450 rpm in 250 s) of the driving engine. The excitation was realized by eight electromagnets as mentioned above. The sloping lines of the vibration with a revolution frequency and its order, i.e., engine order lines, are visible in the diagram. The engine order lines were mainly generated by revolution-dependent excitation by electromagnets and deflections of blades from imbalances and gravitation forces.

The highest amplitudes along these lines (red spots) are achieved at so-called critical speeds when these lines cross vertical branch of the flexural vibration of the wheel. The critical speeds (rpm) can be easily calculated for number of electromagnetic pulses $p = 4x2 = 8$ (twice of number of electromagnet pairs), o order number of pulses, and the resonant frequency (Hz) of the wheel

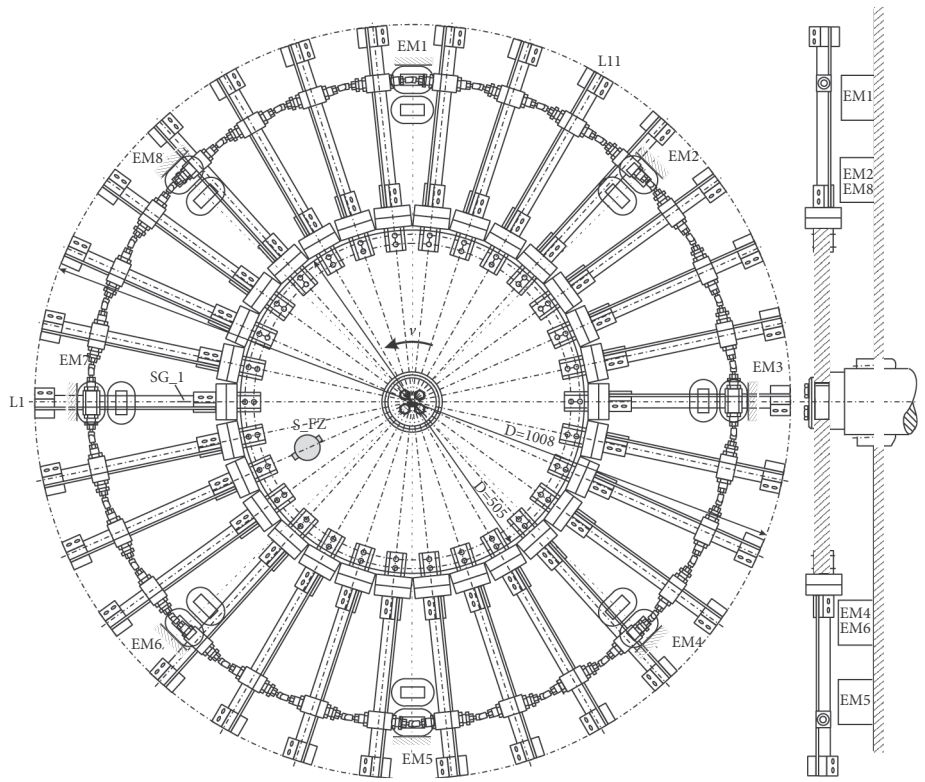

Figure 5: Schematic of the test rig of the bladed wheel.

Table 1: Results of modal analysis of the bladed wheel for open contacts (FEM, experiment).

Eigenfrequency of flexural vibration of the wheel (Hz)										
ND	2		3		4		5		6	
FEM	44.32	44.39	46.14	46.20	47.37	47.42	48.10	48.22	48.54	48.58
Experiment	43.51	—	45.43	45.65	46.59	—	47.08	47.67	48.21	48.66

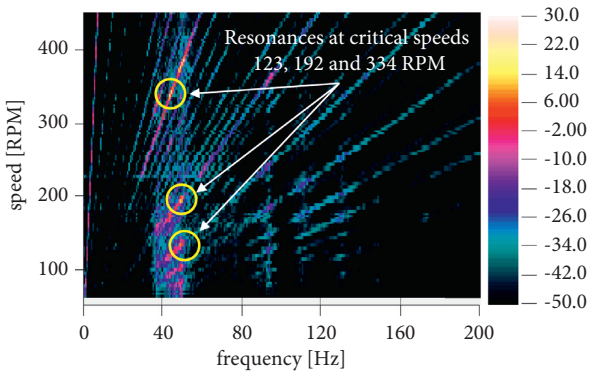

Figure 6: Campbell diagram: 4 pairs of EMs, 2N prestressed contacts. Figure 6 is reproduced from [37].

$$s = \frac{60 f_R}{po}. \quad (1)$$

For evaluation of dry friction damping from a free attenuation, we identified three critical speeds, i.e., 123 ($o = 3$), 192 ($o = 2$), and 334 (o) rpm in the Campbell diagram, so when we know the resonant critical speed, we can calculate back the resonant frequency by equation (1). For evaluation of dry friction damping on the vibration amplitude level, we chose critical speeds at 123 and 334 rpm (Table 2). Since the eigenfrequencies of the wheel change very slightly (up to 1.5 Hz) with the revolution speed, we can identify the mode of vibration, i.e., number of ND, at this critical speed by association with the eigenfrequencies of Table 1.

In the rotary test, the electromagnetic excitation pulled the rotating wheel into the resonance. Then, the excitation was switched off, and the frequencies and damping were evaluated from the amplitude envelope of a free attenuation. The displacement courses of the blade L1 and excitation forces of all pairs of electromagnet pulses were recorded. The records are plotted for the wheel with open contacts, mode 2ND and 331 rpm, as shown in Figure 7.

The displacement of the blade L1 is at the top and the electromagnetic forces F_{emIJ} (see legend) at the bottom. Indexes I and J designate electromagnets that are interconnected in the pairs, and the first index I determines when the electromagnetic excitation is triggered, e.g., both 15 and

Table 2: Parameters of rotary tests for dry friction damping.

No.	p pairs of EM	Max. displacement (mm)	n (rpm)	o order no.	f_R (Hz)	ND
1	8	0.6	334	1	44.53	2
2		0.9				
3		1.2				
4		0.5	123	3	49.20	6
5		0.7				
6		1				

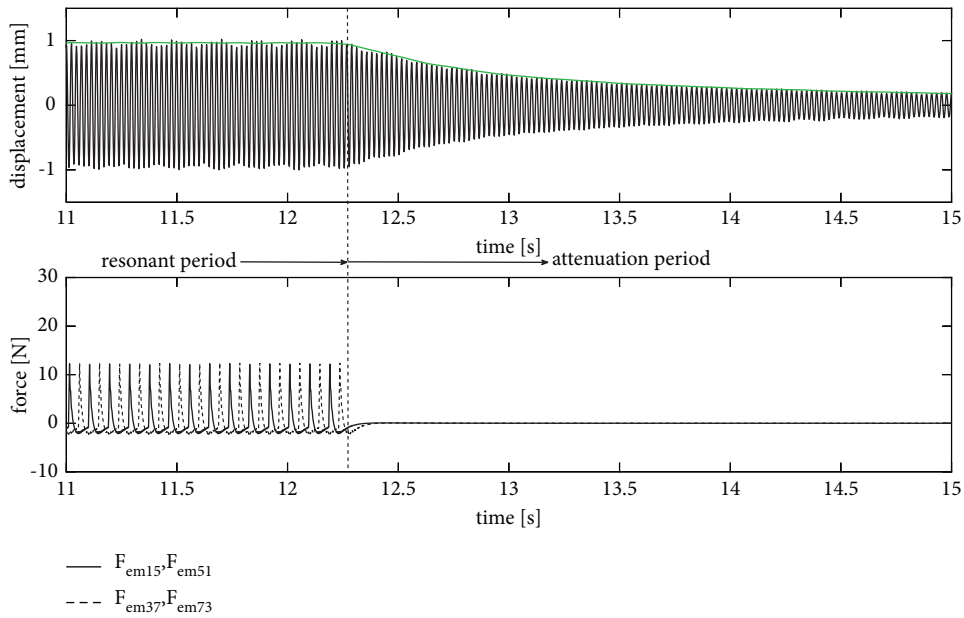

Figure 7: Vibration attenuation: mode 2ND, 331 rpm—open contacts. Figures 7 and 8(a) are reproduced from [37].

51 belong to the same pair (EM1 and EM5), but the excitation comes when blade L1 passes EM1 in case 15 and L1 passes EM5 in case 51. It can be seen that electromagnetic pulses are activated during the resonant vibration period and are switched off during attenuation period. The green line denotes the envelopes of the vibration in the time responses of blade L1. The blade response is almost constant during the resonant period and slowly decreasing during the attenuation period, which proves the low material and aerodynamic damping at this evolution. The cases with prestressed contacts (normal contact force 2 N) and different levels of resonant excitation amplitudes are drawn both for speeds 334 rpm (tests 1–3, Table 2) and 123 rpm (tests 4–6, Table 2) in Figures 8 and 9, respectively, in the same way as in Figure 7.

The fast decrease of the envelope after the resonant period shows the strong effect of dry friction damping on the vibration attenuation. These results were used for evaluation of the dry friction damping effect on different excitation amplitudes and for comparison with numerical results too.

2.4. 3D FE Model with Surface-to-Surface Contacts. Topology of 3D FE model discretization of the wheel is described in the previous chapter. Contacts between the blade were modelled by a "surface-to-surface" method using a pair of contact surface elements TARGET170 and CONTACT174 placed against each other on contact lateral ends of the tie-boss shoulders making 30 contact pairs in the wheel. To detect contact points, the "pinball" search algorithm was used. The augmented Lagrangian method was used to compute contact normal pressures and frictional stresses. Contact surface behavior is modelled as standard unilateral contact, i.e., the normal pressure equals to zero if separation occurs. The friction coupling was modelled by the isotropic Coulomb's law. If the friction stress τ does not exceed the limit friction stress $\tau < \tau_{\text{lim}}$ in the contact surface, where $\tau_{\text{lim}} = \mu_s p$ (μ_s is a static friction coefficient and p is the normal pressure), then the contact is in a state of "sticking." In this state, there is zero sliding between the contact surfaces, and only elastic deformations x_t occur. The contact stiffness k_t is automatically calculated according to the local stiffness of the contact areas by the program. This stiffness estimation was a good fit for our study case, i.e., macroslip movements and smooth surfaces of contacts, since it was not necessary to update its value to improve agreement with experiments.

After the friction stress exceeds the limit by the equivalent friction stress, "sliding" of contact surfaces appears. The size and direction of this sliding are evaluated by the sliding rule using a so-called potential of friction flow.

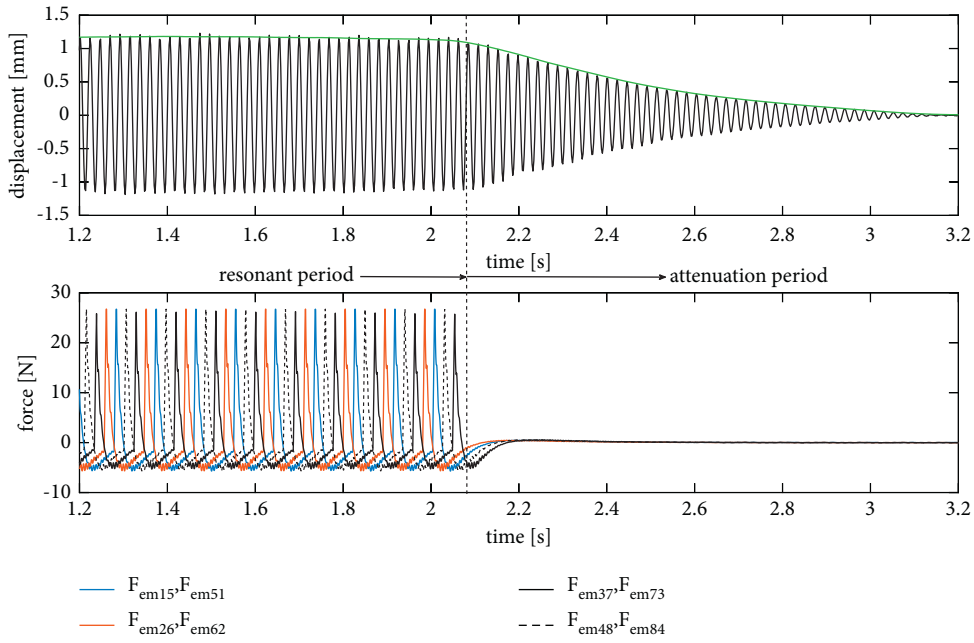

(a)

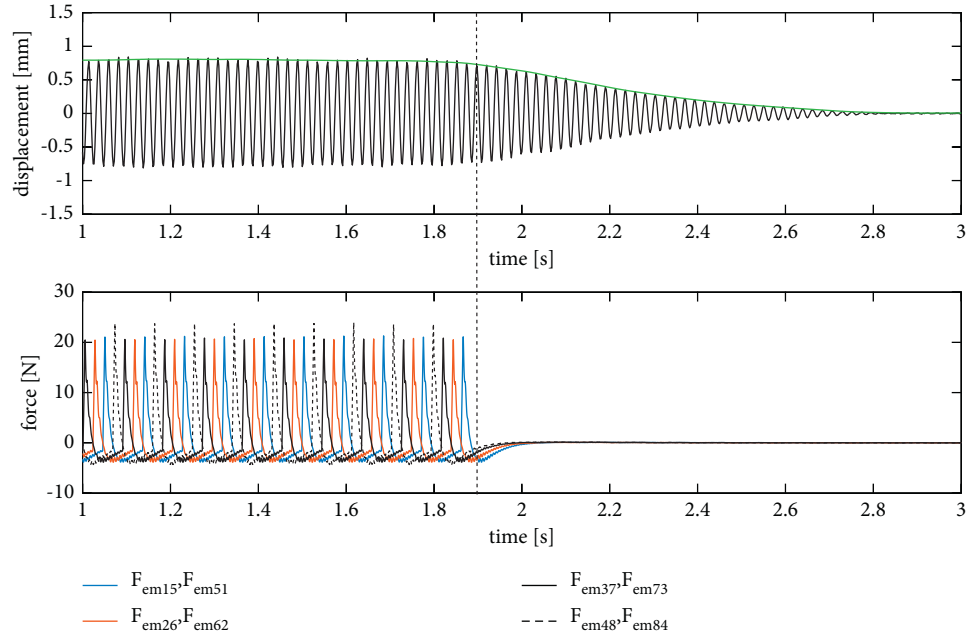

(b)

Figure 8: Continued.

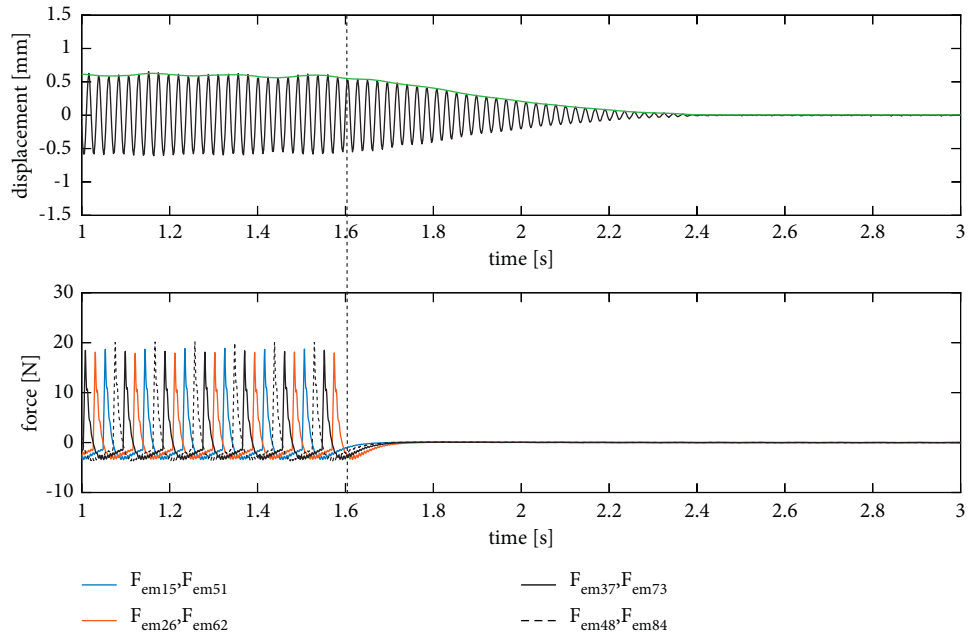

(c)

Figure 8: Vibration attenuation: mode 2ND, 334 rpm contact prestress 2 N. (a) Test no. 3. (b) Test no. 2. (c) Test no. 1.

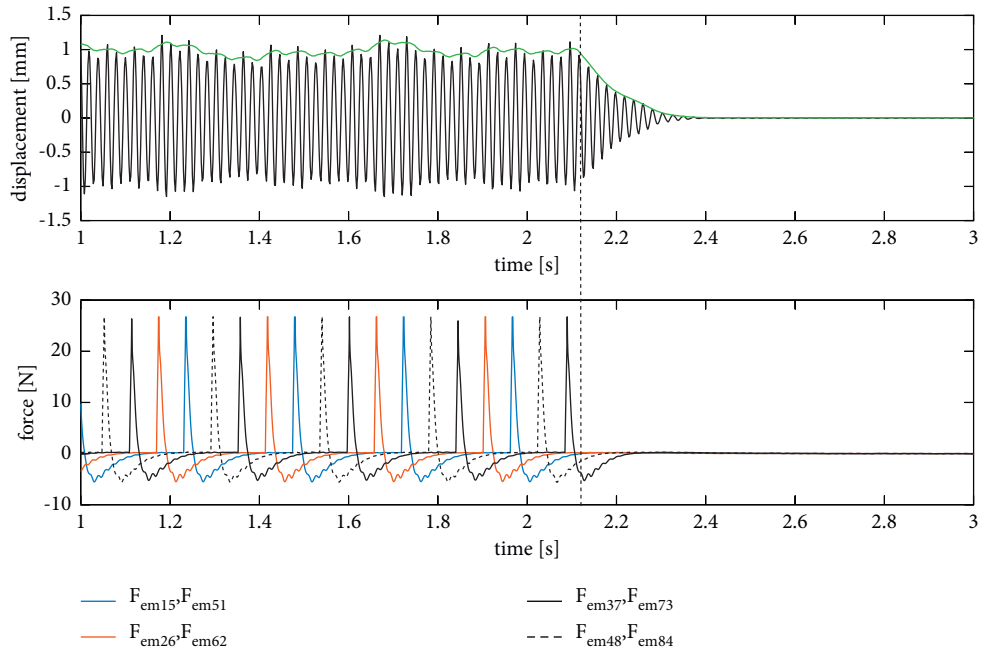

(a)

Figure 9: Continued.

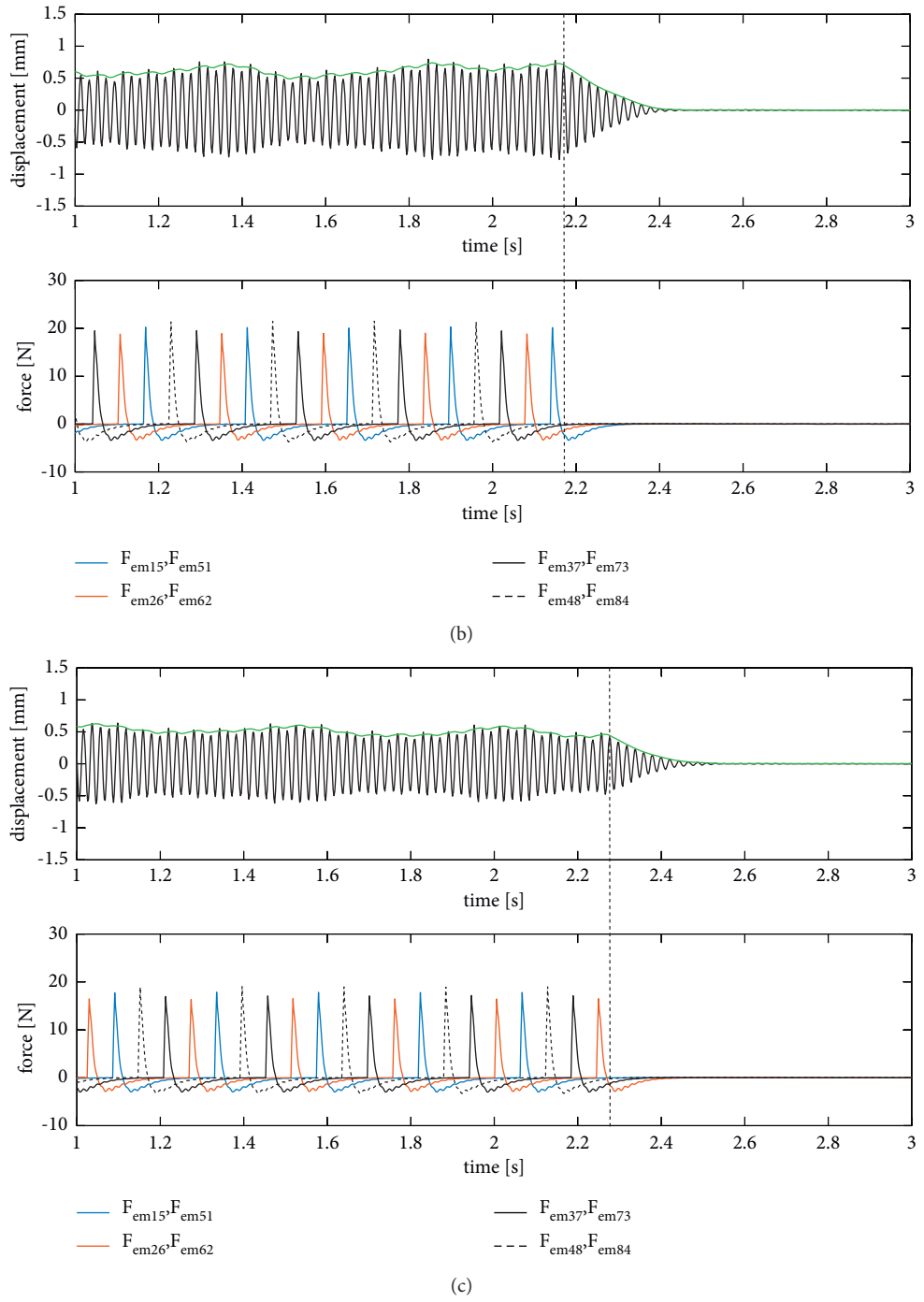

Figure 9: Vibration attenuation: mode 6ND, 123 rpm contact prestress 2 N. (a) Test no. 6. (b) Test no. 5. (c) Test no. 4.

For a description of the friction coefficient μ, the following dependence on relative velocity v_{rel} is considered:

$$\mu = \mu_d\left[1 + \left(\text{FACT} - 1\right)e^{\left(-\text{DC}v_{\text{rel}}\right)}\right], \tag{2}$$

where $\text{FACT} = \mu_s/\mu_d$, μ_d represent the dynamic friction coefficients, and DC represents the decay coefficient. Values $\mu_s = 0.4$, $\mu_d = 0.2$, and $\text{DC} = 4$ were used for the computation of the dynamics of the wheel, as shown in Figure 10.

The prestress in contacts was modelled by contact surface offset $1e-5$ m with a resulting normal contact force of 2.4 N. Setting of the boundary and initial condition for transient analysis of the wheel is described in the next chapter.

A full solver for the unsymmetrical task solved the transient responses with the Newmark integration method and time step $5e-6$ s. The Newmark parameter $\gamma = 0.5$ was set for numeric stabilization reasons. The damping ratio

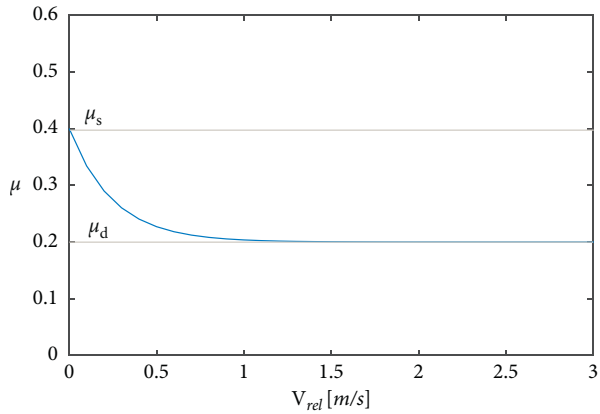

FIGURE 10: Dependence of friction coefficient on the relative velocity. Figure 10 is reproduced from [37].

0.1% was imposed as the steel material and other construction damping.

3. HPC Computational Strategy

Due to long computation time of nonlinear transient solution of wheel response, we had to deal with a computational strategy for damping evaluation. To eliminate the long resonant run-up to steady state before a free attenuation as performed at experiments, the resonant state was defined directly by the input initial conditions, i.e., the displacements of wheel were set as a chosen eigenmode with zero velocities. The term "free" means that the dynamic response for damping evaluation deals with an unforced vibration attenuation.

The applied computational strategy can be divided into three steps.

(1) Modal analysis of the wheel with open contacts for identification of modal vectors. Creation of the excitation force vector from the chosen modal vector according to required number of nodal diameters (ND). The forces act in preselected nodes. It provides affinity of the excitation vector to the chosen eigenmode.

(2) Before the transient solution of free attenuation from the prescribed initial displacements, we have to achieve a static solution of the wheel deformation under the excitation vector ascertained in step 1.

(3) Transient solution of vibration attenuation from initial displacements achieved in step 2. External forces and velocities are set to zero.

The integration period 0.1 s (corresponds to 20000 integration steps) of the vibration attenuation by ANSYS parallel computing required about 40000 core hours of computational resources of the supercomputer Salomon. If the resonant run-up was included, the task requirement would be multiple.

3.1. Numerical Results. Due to HPC time demanding computations of the transient responses of the wheel, we aimed at study cases for which experimental data were available and could be directly compared with the experiment. Namely, we dealt with the two resonant attenuations for 2ND and 6ND modes of vibration.

The 2ND and 6ND modes with open contacts were precomputed for creation of the excitation vector. From the distribution of displacements of the modal vector, the affinity force vectors *Fx*, *Fy*, and *Fz* denoted by red vectors in Figures 11(a) and 12(a), respectively, in selected nodes of the wheel were added. For our case, the force vectors were specified at two nodes of the tie-boss prism of each blade around the circumference. The total static displacements (m) of the wheel computed for the 2ND, 6ND, and their modal force distributions are shown in Figures 11(b) and 12(b), respectively. The ascertained deformation modes were used as initial displacement conditions for the next transient analysis.

Since the attenuation is monotonic and the mode of vibration holds on during all calculation periods, the response of the wheel is presented here as time characteristics of displacements of selected nodes of target-contact pairs of the contact A (Figures 13(a), 13(b), 14(a), and 14(b)) and the contact B (Figures 13(c), 13(d), 14(c), and 14(d)) denoted in Figure 3(b). Amplitude envelopes are plotted in red (upper envelope) and green (bottom envelope) for displacements of node N165136. One can see almost linear decrease of the amplitudes typical for dry friction damping modelled by Coulomb's law. To show the complex relative motion of the contact surfaces during vibration by 2ND and 6ND modes, trajectories of blade motions at the same contact-target pair nodes as before are shown in Figures 15 and 16, respectively. The trajectories correspond to one vibration period defined by blue frames in Figures 13 and 14. The graph shows that there is nonparallel relative motion of the contact surfaces that causes variable contact states as to the localization of contact areas and value of contact normal stresses during vibration. As to the localization of contact areas, very often edge contacts arise as shown in a detail of three blades for one selected integration time, i.e., 0.096745 s for 2ND mode (Figure 17) and 0.035995 s for 6ND mode (Figure 18). The contact state picture shows which areas are in a sliding contact (sliding) and which are contact open (near contact state).

3.2. Comparison with Experiment. To compare the numerical results with the experimental data, we inserted all results into the aggregate graph of amplitude attenuations (Figure 19). The envelopes corresponding to resonant attenuation of the 2ND mode evaluated from experiment is denoted by light blue and 6ND by violet. There are three tests (tests 1–3) distinguished by the amplitude level of the resonant attenuation for each mode. The numerical FE envelopes are denoted by blue and red lines for 2ND and 6ND modes (upper envelope from Figure 14(c)), respectively. In case of 2 ND, there were two separate tasks with (A) higher (upper envelope from Figure 13(c)) and (B) lower initial amplitudes (Pešek et al. [39]), and therefore, the black line is interrupted. For a better comparison with the experimental data, they were shifted in time and pinned to experimental

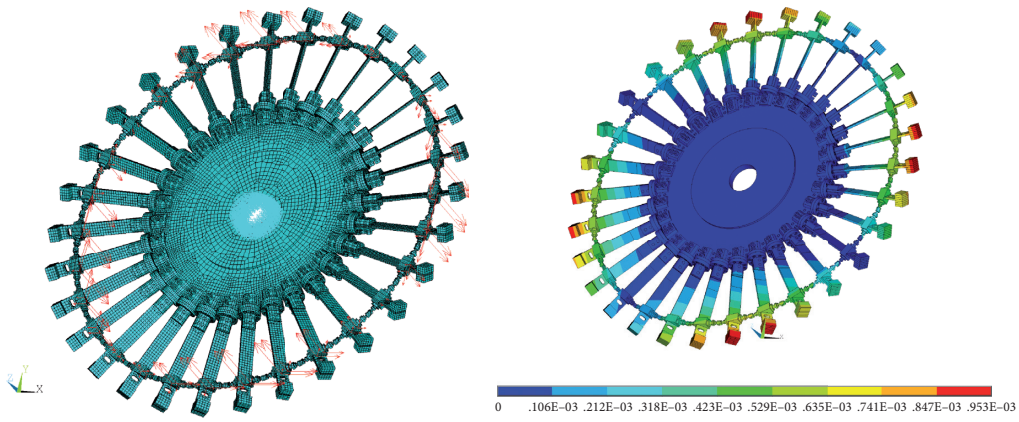

(a) (b)

FIGURE 11: (a) Distribution of modal forces around the wheel (red vector). (b) Contour maps of initial displacements (m) of the wheel—2ND mode.

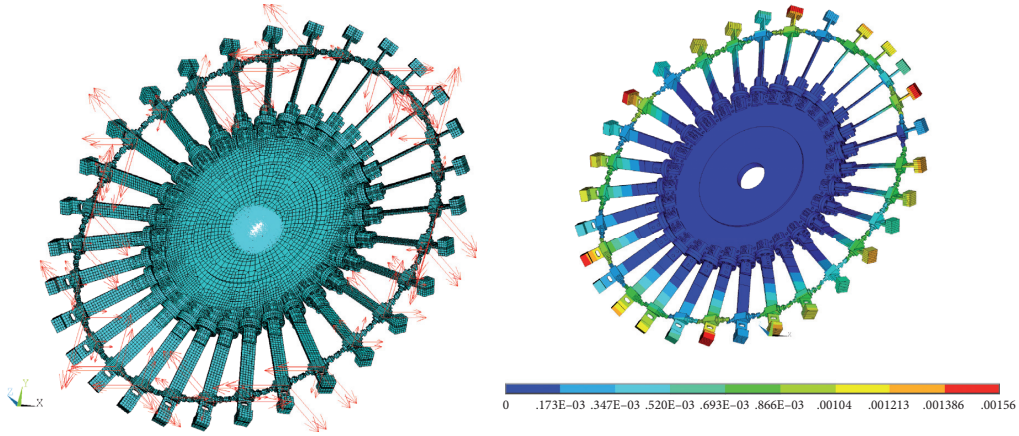

(a) (b)

FIGURE 12: (a) Distribution of modal forces around the wheel (red vector). (b) Contour maps of initial displacements (m) of the wheel—6ND mode.

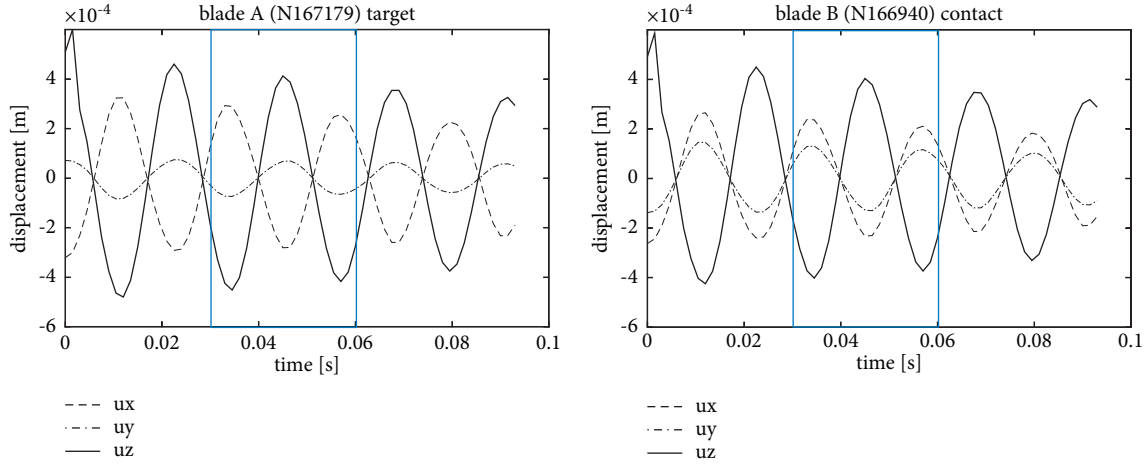

(a) (b)

FIGURE 13: Continued.

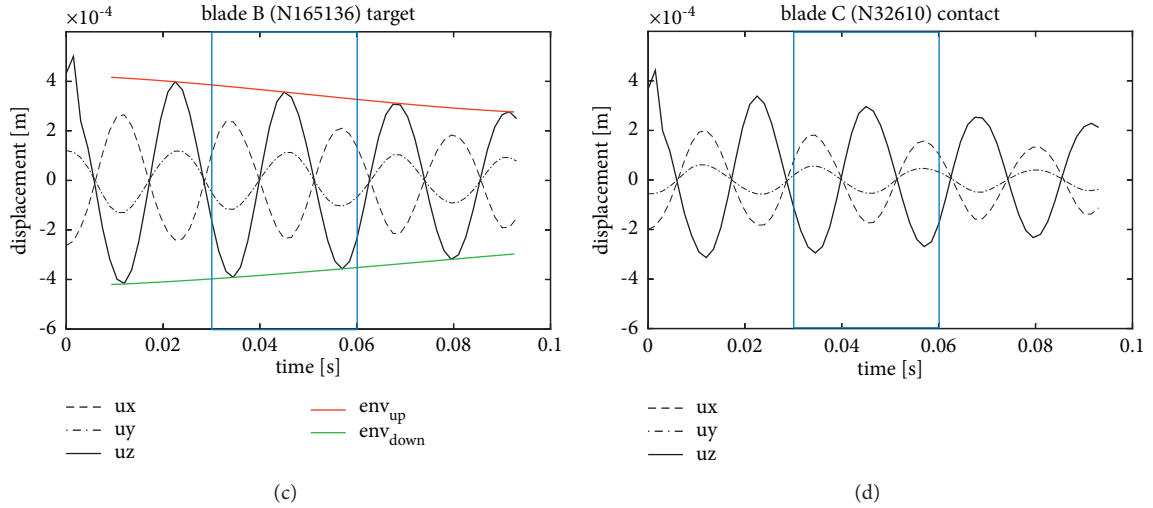

Figure 13: Time characteristics of displacements of blades BA, BB, and BC in nodes of target-contact pairs: (a)-(b) contact (A); (c)-(d) contact (B). Amplitude envelopes are denoted by red and green lines—2 ND mode.

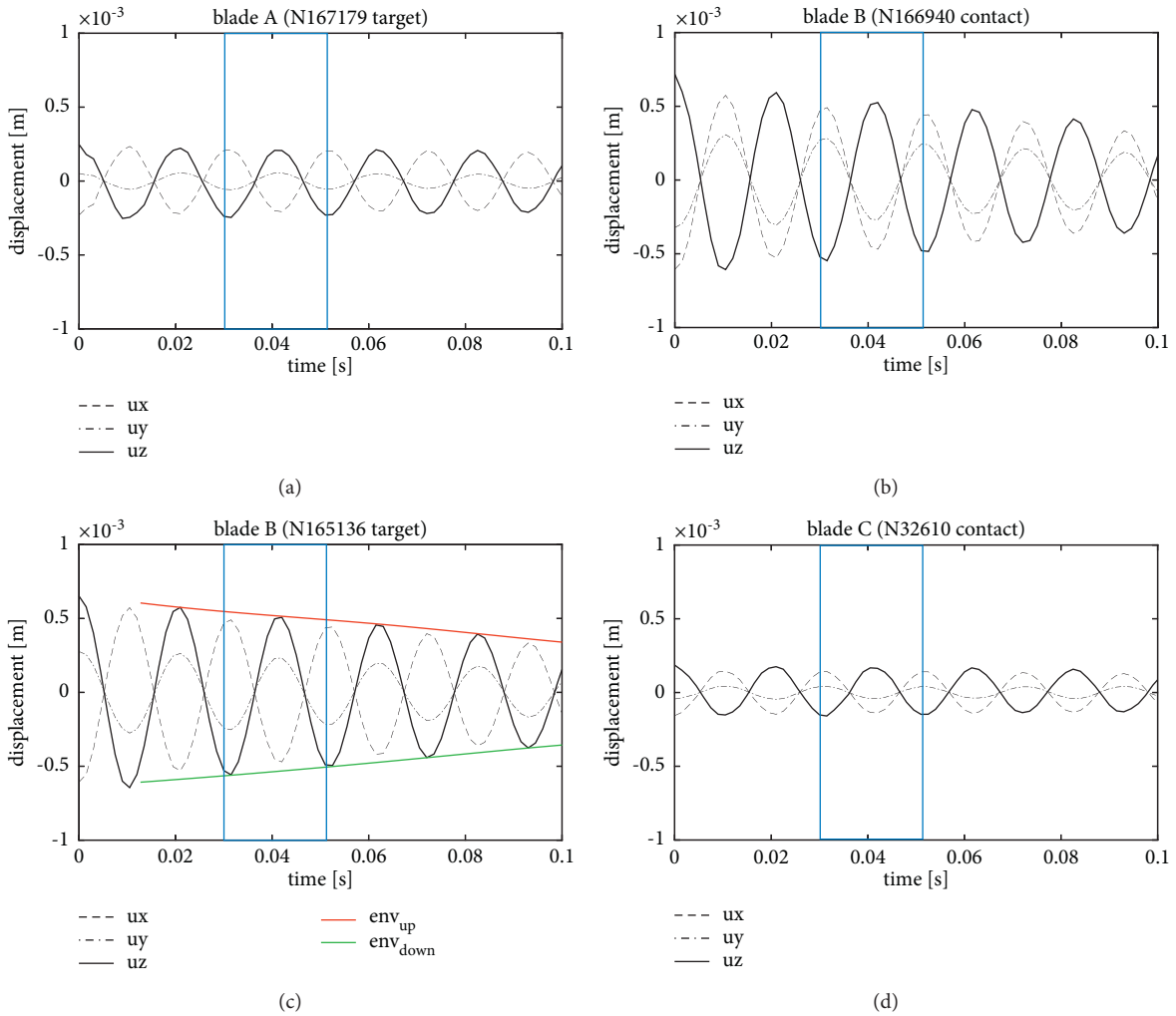

Figure 14: Time characteristics of displacements of blades BA, BB, and BC in nodes of target-contact pairs: (a)-(b) contact (A); (c)-(d) contact (B). Amplitude envelopes are denoted by red and green lines—6ND mode.

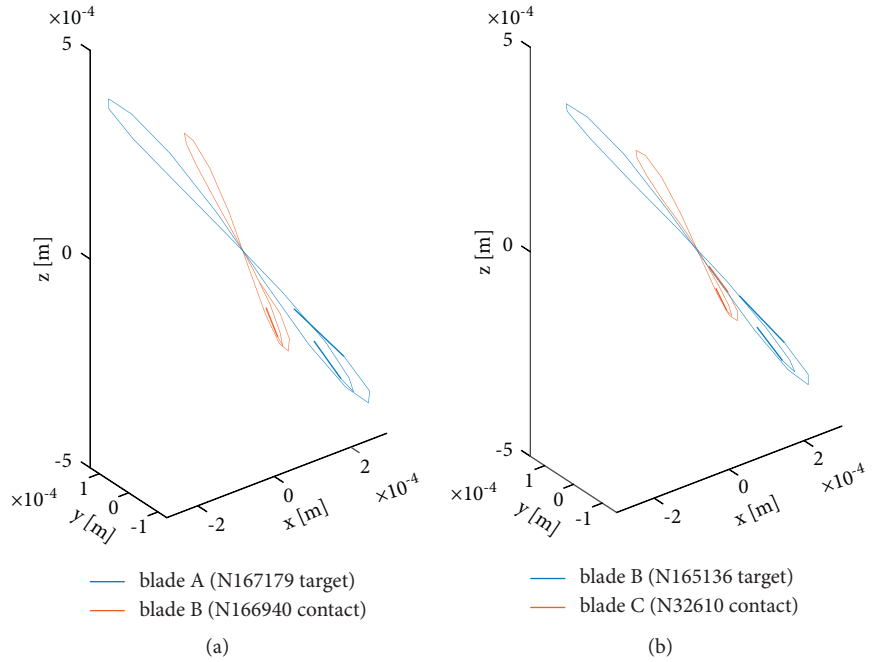

Figure 15: Trajectories of blade motions at contact-target pair nodes in the middle of contact surfaces—2ND mode.

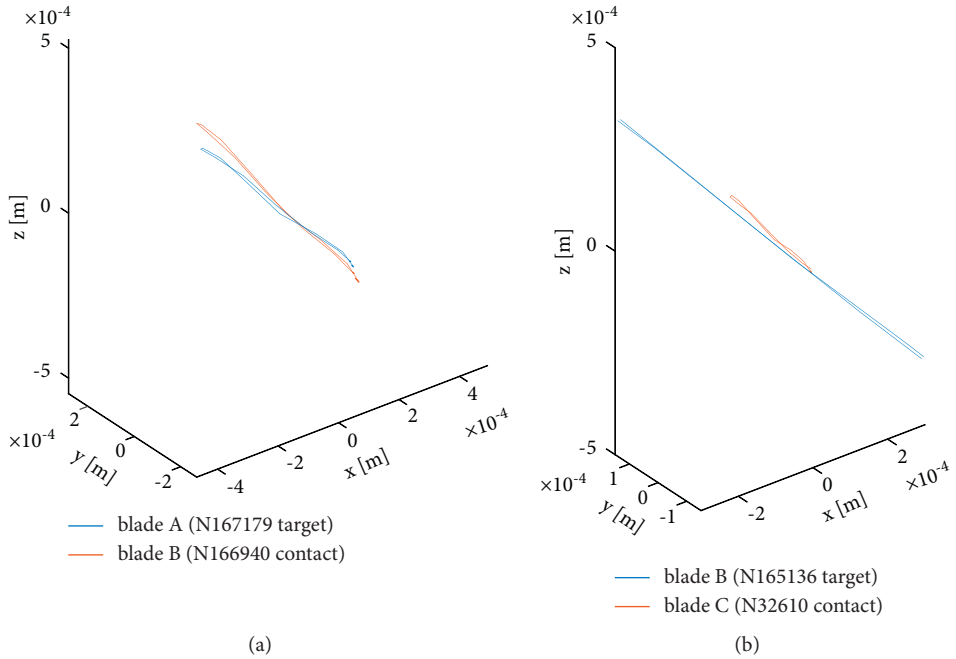

Figure 16: Trajectories of blade motions at contact-target pair nodes in the middle of contact surfaces—6ND mode.

data and do not start from time zero. Marks on the lines denote the peaks of the amplitude of harmonic attenuation.

The graph shows that the numerical results match very well to the experimental data in the range of computed displacements (up to 0.5 mm) of the blades. The higher slope of 6ND than 2D envelopes indicates that a higher damping effect can be expected on the mode with a higher number of ND at comparable absolute displacements due to higher relative motions in contacts. The damping ratios evaluated from logarithmic decrement of the FEM envelopes yields 1.2% for 2ND and 2.2% for 6ND. Experimental data show more pronounced dependence of amplitude decay on higher absolute amplitudes (above 0.5 mm). It shows a slightly higher nonlinear effect at friction contacts. It may be caused by, e.g., different characters of friction coefficient at higher relative velocities or more nonlinear behavior in contact of the experimental model due to production inaccuracies.

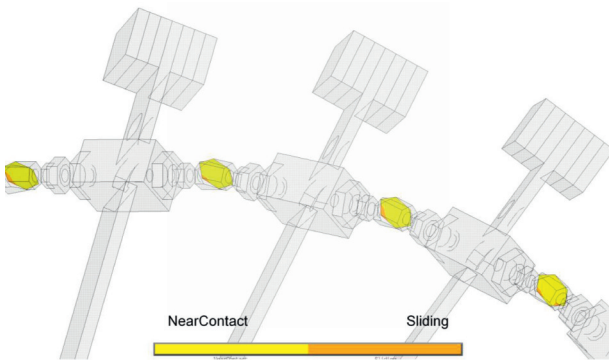

Figure 17: Detail of contact statuses (near contact and sliding) at tie-boss couplings (detail) at 0.096745 s—2ND mode.

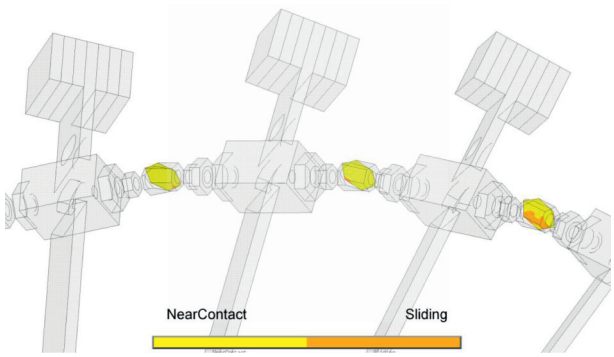

Figure 18: Detail of contact statuses (near contact and sliding) at tie-boss couplings 0.035995 s—6ND mode.

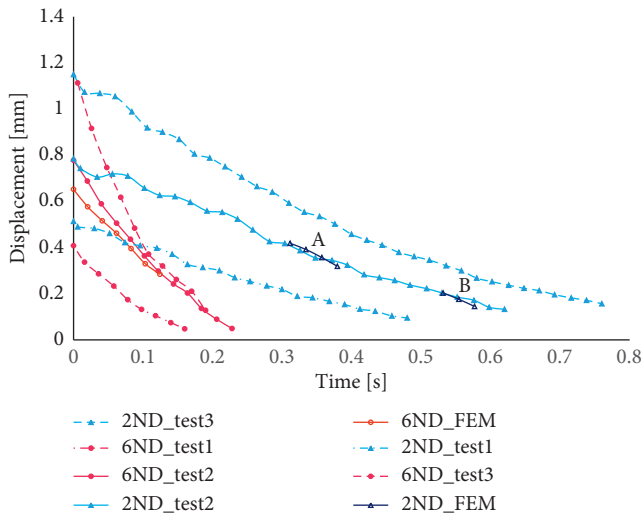

Figure 19: Envelopes of the vibration attenuation for 2ND an 6ND modes—experimental and FEM results.

4. Conclusion

In the study, dry friction interblade damping of the bladed disk was solved by the three-dimensional FE model with the surface-to-surface dry friction contact model. It enabled to model time and space (spot and edge contacts) variant contact states and analyze the dry friction effect in such geometrically complex structures as the bladed disk with interblade contacts. The damping study aimed at the case when sliding states prevail in the contact (macroslip motion) which can occur at larger blade displacements. This solution, however, due to nonlinear solution of the dynamics, leads to time-consuming computations. Thanks to high performance computation (HPC) facilities; these tasks are, nowadays, computationally more feasible. Our computations were performed using 24 processors per 5 nodes on the supercomputer Salomon in the Centre IT4Innovation with 2PFLOPS Rpeak. Due to nonlinear solution of the dynamics and therefore long computation times, a computational strategy for more effective damping evaluation was proposed. Using our computational strategy for damping evaluation, i.e., the damping effect is evaluated from the solution of free attenuation at predefined initial conditions; the net computational time of the 6ND mode case was lowered to 7 days.

To compare and validate numerical results experimentally, the physical model of the disk with interblade tie-boss's contacts was built and tested on the rig under revolution. It was shown that the numerical results match very well to the experimental data in the range of computed displacements and modes of vibration of the blades.

The study yields very valuable results and shows that the proposed numerical 3D modelling of the bladed disk with dynamical surface to surface contacts is perspective for assessment of damping behavior of the bladed wheels when adhesion in contacts is exceeded and contacts get into macroslip relative motion. It could help to design more effective interblade damping couplings, such as their placement, mass and stiffness distribution, and tilting of contact areas, with respect to the danger excitation of the wheel vibration modes.

Data Availability

The data or information used for the study were generated from the cited literature or our own resources. It is described herein how data were obtained. More information can be gained directly upon request to the authors. As to applicability, the study yields very valuable results and shows that proposed numerical 3D modelling of the bladed disk with dynamical surface-to-surface contacts is perspective for assessment of damping behavior of the bladed wheels. It could help to design more effective interblade damping couplings with respect to the danger excitation of the wheel vibration mode.

Conflicts of Interest

The authors declare that they have no conflicts of interest.

Acknowledgments

This work was supported by the research project of the Czech Science Foundation "Study of dynamic stall flutter instabilities and their consequences in turbomachinery

application by mathematical, numerical, and experimental methods" (20-26779S). The HPC calculations were supported by the Czech Ministry of Education, Youth, and Sports from the Large Infrastructures for Research, Experimental Development, and Innovations project IT4Innovations National Super-Computing Center (LM2015070).

References

[1] L. Pešek, L. Půst, P. Šnábl, V. Bula, M. Hajžman, and M. Byrtus, "Dry-friction damping in vibrating systems," in *Theory and Application to the Bladed Disc Assembly, Chapter of the Book: Nonlinear Structural Dynamics and Damping*, J. C. Jáuregui, Ed., Springer Book, Germany, 2019.

[2] N. Bachschmid, S. Bistolfi, M. Ferrante, P. Pennacchi, E. Pesatori, and M. Sanvito, "An investigation on the dynamic behaviour of blades coupled by shroud contacts," in *Proceedings of the SIRM 2011*, Darmstadt, Germany, December 2011.

[3] W. Gu, Z. Xu, and Y. Liu, "A method to predict the non-linear vibratory response of bladed disc system with shrouded dampers," *Proceedings of the Institution of Mechanical Engineers - Part C: Journal of Mechanical Engineering Science*, vol. 226, no. 6, pp. 1620–1632, 2012.

[4] B. Santhosh, S. Narayanan, and C. Padmanabhan, "Nonlinear dynamics of shrouded turbine blade system with impact and friction," *Applied Mechanics and Materials*, vol. 706, pp. 81–92, 2014, ISSN 16609336.

[5] E. P. Petrov and D. J. Ewins, "Effects of damping and varying contact area at blade-disk joints in forced response analysis of bladed disk assemblies," *Journal of Turbomachinery*, vol. 128, no. 2, pp. 403–410, 2006.

[6] E. P. Petrov and D. J. Ewins, "Advanced modelling of underplatform friction dampers for analysis of bladed disc vibration," *Proc of the ASME Turbo Expo*, vol. 5, pp. 769–778, 2006.

[7] D. Botto, S. Zucca, S. Pavone, and M. M. Gola, "Parametric study of the kinematic behaviour of the underplatform damper and correlation with experimental data," *Proc of ISMA*, vol. 1-8, pp. 1039–1053, 2008.

[8] M. M. Gola and T. Liu, "A direct experimental-numerical method for investigations of a laboratory under-platform damper behavior," *International Journal of Solids and Structures*, vol. 51, no. 25-26, pp. 4245–4259, 2014, ISSN 00207683.

[9] S. Zucca and C. M. Firrone, "Nonlinear dynamics of mechanical systems with friction contacts: coupled static and dynamic Multi-Harmonic Balance Method and multiple solutions," *Journal of Sound and Vibration*, vol. 333, no. 3, pp. 916–926, 2014.

[10] L. Pesaresi, L. Salles, A. Jones, J. S. Green, and C. W. Schwingshackl, "Modelling the nonlinear behaviour of an underplatform damper test rig for turbine applications," *Mechanical Systems and Signal Processing*, vol. 85, pp. 662–679, 2017.

[11] A. Francavilla and O. C. Zienkiewicz, "A note on numerical computation of elastic contact problems," *International Journal for Numerical Methods in Engineering*, vol. 9, no. 4, pp. 913–924, 1975.

[12] P. Wriggers, T. Vu Van, and E. Stein, "Finite element formulation of large deformation impact-contact problems with friction," *Computers & Structures*, vol. 37, no. 3, pp. 319–331, 1990.

[13] J. C. Simo and T. A. Laursen, "An augmented Lagrangian treatment of contact problems involving friction," *Computers & Structures*, vol. 42, no. 1, pp. 97–116, 1992.

[14] W. Sextro, *Dynamical Contact Problems with Friction*, Springer, Berlin, Germany, 2007.

[15] J. Awrejcewicz and Y. Pyr'yev, *Nonsmooth Dynamics of Contacting Thermoelastic Bodies*, Springer, Berlin, Germany, 2009.

[16] L. Pešek, F. Vaněk, J. Veselý, V. Bula, and J. Cibulka, "Design of test excitation of traveling waves of rotating bladed wheels with multipoint electromagnetic excitation," in *Proceedings of the SIRM 2011*, Darmstadt, Germany, December 2011.

[17] P. Pennacchi, S. Chatterton, N. Bachschmid, E. Pesatori, and G. Turozzi, "A model to study the reduction of turbine blade vibration using the snubbing mechanism," *Mechanical Systems and Signal Processing*, vol. 25, no. 4, pp. 1260–1275, 2011.

[18] L. Pešek and L. Půst, "Blade couple connected by damping element with dry friction contacts," *Journal of Theoretical and Applied Mechanics*, vol. 52, no. 3, pp. 815–826, 2014.

[19] L. Pešek, M. Hajžman, L. Půst, V. Zeman, M. Byrtus, and J. Brůha, "Experimental and numerical investigation of friction element dissipative effects in blade shrouding," *J. Nonlinear Dynamics*, vol. 79, no. 3, pp. 1711–1726, 2015.

[20] V. Zeman, M. Byrtus, and M. Hajžman, "Harmonic forced vibration of two rotating blades with friction damping," *Engineering Mechanics*, vol. 17, no. 3/4, pp. 187–200, 2010.

[21] K. Magnus and P. K. Schwingungen, *Teubner Studienbücher Mechanik*, Vol. 5, Auflage, Stuttgart, 1997.

[22] A. Zmitrowicz, "A vibration analysis of a turbine blade system damped by dry friction forces," *International Journal of Mechanical Sciences*, vol. 23, no. 12, pp. 741–761, 1981.

[23] C. Pierre, A. A. Ferri, and E. H. Dowell, "Multi-harmonic analysis of dry friction damped systems using an incremental harmonic balance method," *Journal of Applied Mechanics*, vol. 52, no. 4, pp. 958–964, 1985.

[24] A. A. Ferri and E. H. Dowell, "Frequency domain solutions to multi-degree-of-freedom, dry friction damped systems," *Journal of Sound and Vibration*, vol. 124, no. 2, pp. 207–224, 1988, ISSN 0022460X.

[25] E. P. Petrov and D. J. Ewins, "State-of-the-art dynamic analysis for non-linear gas turbine structures," *Proceedings of the Institution of Mechanical Engineers - Part G: Journal of Aerospace Engineering*, vol. 218, no. 3, pp. 199–211, 2004.

[26] E. P. Petrov, "Method for sensitivity analysis of resonance forced response of bladed disks with nonlinear contact interfaces," *Journal of Engineering for Gas Turbines & Power*, vol. 131, no. 2, Article ID 022510, 2009.

[27] K. Y. Sanliturk, M. Imregun, and D. J. Ewins, "Harmonic balance vibration analysis of turbine blades with friction dampers," *Journal of Vibration and Acoustics*, vol. 119, no. 1, pp. 96–103, 1997.

[28] D. Suss, M. Jerschl, and K. Willner, "Adaptive harmonic balance analysis of dry friction damped systems," *Nonlinear Dynamics* in *Proceedings of the 34TH IMAC Book Series: Conference Proc of the Society for Experimental Mechanics Series*, vol. 1, pp. 405–414, Jacksonville, September 2016.

[29] C. W. Schwingshackl, E. P. Petrov, and D. J. Ewins, "Validation of test rig measurements and prediction tools for friction interface modelling," *Turbo Expo: Power for Land, Sea, and Air*, vol. 44014, 2010.

[30] J. Voldřich, J. Lazar, P. Polach, and J. Voldřich, "Finding the stiffnesses of interface contact elements for the computational model of steam turbine blading," in *Proceedings of the ASME IDETC/CIE 2017*, vol. 58226, Cleveland, USA, 2017.

[31] N. Bachschmid, P. Pennacchi, and M. Lurati, "Combining mistuning and snubbing in bladed disks of turbomachinery," *Proc of ISMA*, vol. 1-8, pp. 1009–1022, 2008.

[32] Y. Yamashita, K. Shiohata, T. Kudo, and H. Yoda, "Vibration characteristics of a continuous cover blade structure with friction contact surfaces of a steam turbine," in *Proceedings of the 10th International Conference on VIRM*, pp. 323–332, Woodhead Publishing, London, UK, September 2012.

[33] L. Pešek, L. Půst, F. Vaněk, V. Bula, and J. Cibulka, "Inter-slip damping of twisted blades in opposed bundles under rotation," in *Proceedings of the 10th VIRM, Institution of Mechanical Engineers*, vol. 10, September 2012.

[34] L. Pešek, L. Půst, V. Bula, and J. Cibulka, "Investigation of dry friction effect of shroud damping wire on model test bladed wheel," in *Proceedings of the ASME IDETC/CIE 2013*, vol. 7, Article ID DETC2013-12851, Portland, USA, 2013.

[35] L. Pešek, L. Půst, V. Bula, and J. Cibulka, "Numerical analysis of dry friction damping effect of tie-boss couplings on three blade bundle," in *Proceedings of the ASME IDETC/CIE 2017*, vol. 7, Cleveland, USA, 2017.

[36] R. Drozdowski, L. Volker, D. Hafele, and D. M. Vogt, "Experimental and numerical investigation of the nonlinear vibrational behavior of steam turbine last stage blades with friction bolt damping elements," in *Proceedings of the ASME Turbo Expo 2015*, vol. 8, Canada, 2015.

[37] L. Pešek, P. Šnábl, P. Šulc, L. Půst, and V. Bula, "Modelling of non-linear dynamics of bladed model disk with dry-friction contacts in tie-bosses," in *IFToMM World Congress on Mechanism and Machine Science, Published in Advances in Mechanism and Machine Science*, pp. 3429–3438, Springer Book, Germany, 2019, Available at https://link.springer.com/book/10.1007%2F978-3-030-20131-9.

[38] L. Pešek, L. Půst, P. Šulc, P. Šnábl, and V. Bula, "Stiffening effect and dry-friction damping of bladed wheel model with "tie-boss" couplings - numerical and experimental investigation," *Book chapter of Mechanisms and Machine Science*, vol. 62, pp. 148–162, 2019.

[39] L. Pešek, L. Půst, V. Bula, and J. Cibulka, "HPC FEM calculations for damping estimation of bladed disk with dry-friction contacts," in *Proceedings of the ASME IDETC/CIE 2020*, vol. 5, St.Louis, USA, 2020.

[40] D. J. Segalman, T. Paez, D. Smallwood, A. Sumali, and A. Urbina, *Status and Integrated Road-Map for Joints Modeling Research*, Sand Report, SAND2003-0897, Albuquerque, NM, 2003.